PERGAMON

EFFECT OF CRYSTALLINITY ON THE IMPACT TOUGHNESS OF A La-BASED BULK METALLIC GLASS

N. NAGENDRA[1], U. RAMAMURTY[1]†, T. T. GOH[2] and Y. LI[2]

[1]School of Mechanical and Production Engineering, Nanyang Technological University, Singapore 639798 and [2]Department of Materials Science, National University of Singapore, Singapore 119260

Abstract—The influence of crystallinity on the ductile–brittle transition in a bulk lanthanum-based metallic glass was investigated. The degree of crystallization in the metallic glass, which was processed through the arc-melting and water-quenching route, was systematically altered by varying the annealing time above the glass transition temperature. The resulting amorphous/crystalline microstructures were characterized by XRD, DSC, and TEM techniques. Instrumented impact test results show a significant decrease, by $\sim 90\%$, in impact toughness with the introduction of a small percentage of crystallinity. This decrease in toughness was also associated with a distinct change in fracture morphology, from a ductile *vein-type* fracture in the bulk glass to intergranular cleavage fracture in the crystalline material. The observed fracture transition was rationalized by recourse to the mechanism of stress relaxation due to viscous flow. For this purpose, variations in elastic modulus and dynamic viscosity with respect to the crystallinity were measured using a dynamic mechanical analyzer. The characteristic relaxation times were computed from the viscosity data and were used to explain the ductile–brittle transition. Microscopic mechanisms responsible for the fracture transition are also discussed. © *2000 Acta Metallurgica Inc. Published by Elsevier Science Ltd. All rights reserved.*

Keywords: Toughness; Metallic glasses; Embrittlement; Composites; Shear bands

1. INTRODUCTION

Recent innovations in processing metallic glasses in bulk form have made them candidate materials for many potential structural applications wherein their unique mechanical properties can be exploited. While a number of glass-forming systems have been investigated for their mechanical properties and micromechanisms of failure, Zr-based alloys (Zr–Ti–Cu–Ni–Be and Zr–Al–Cu–Ni) have received particular attention [1–15]. These alloys exhibit insignificant plastic strain at failure but show large elastic strains of up to $\sim 2\%$. In addition, their fracture properties, under quasi-static, cyclic, and impact loading conditions, were found to be comparable with that of high-strength steels and aluminum alloys [16–18].

Recently, nanocrystalline (crystal size less than 10 nm)-amorphous matrix composites were processed by controlled annealing of amorphous alloys between the glass transition temperature and the crystallization temperatures [19, 20]. The elastic modulus, E, and tensile strength, σ_u, of the compo-

sites were reported to increase with increasing crystal volume fraction, χ, whereas the strain to failure, ε_u, remains unchanged in the Zr–M(Ti, Nb, Pd)–Al–Ni–Cu system [21]. However, a further increase in χ after a certain critical value leads to a precipitous drop in both the σ_u and ε_u, indicating a ductile–brittle transition [21]. Gilbert *et al.* [12] have reported a 50-fold reduction in the fracture toughness of a bulk metallic glass alloy $Zr_{41.2}Ti_{13.8}Cu_{12.5}Ni_{10}Be_{22.5}$ upon partial crystallization (with $\chi \sim 5\%$) or full crystallization. Research work on metallic glass ribbons also indicates severe embrittlement upon crystallization of amorphous metals, which shows that the presence of nanocrystalline phases can severely degrade their ductility, fracture toughness, and fatigue crack growth resistance [12, 22–24]. However, a detailed understanding of the micromechanisms responsible for the embrittlement is yet to be developed.

The development of nanocrystalline-amorphous composites has raised issues such as (i) the volume fraction and types of crystalline phases acceptable in the amorphous matrix without being detrimental to the mechanical performance and (ii) the deformation mechanisms controlling the composite's properties. The research reported in the present

---

† To whom all correspondence should be addressed.

paper was initiated to address some of these issues. In addition, an objective that is more fundamental in nature, is the following. In principle, with increasing amount of crystallization, the energy dissipated through viscous deformation of glass phase should decrease. At the same time, dislocation-based energy absorption mechanisms can become operative and may contribute increasingly to the overall impact toughness†. Thus, these two competing effects should lead a minimum in fracture toughness at a particular crystallization level. The validity of this hypothesis needs to be verified as it can greatly aid in the design of better nanocrystalline-amorphous composites.

A bulk metallic glass based on the La–Al–TM (TM = Co, Ni, Cu) system has been chosen to study the influence of crystallization on the impact toughness by the glass. Controlled amounts of crystallinity have been induced in the glass by varying the annealing time and the relative change in impact toughness is measured in an instrumented impact tester. The toughness and the resultant fracture morphology have been shown to be dependent on the viscous deformation behavior of the glass. The inherent material property of significance was found to be the characteristic relaxation time, which is in turn dependent on its dynamic elastic modulus and viscosity.

2. EXPERIMENTAL PROCEDURE

The ingots were prepared by arc-melting a mixture of 99.9% pure La, 99.997% pure Al, 99.999% pure Cu, 99.95% pure Ni and 99.5% pure Co metals in a purified argon atmosphere [25, 26]. Bulk amorphous alloys with a nominal composition of $La_{55}Al_{25}Cu_{10}Ni_5Co_5$ and diameter of 4 mm were prepared by remelting the master ingots in sealed quartz tubes (in argon atmosphere) at a temperature of 973 K for 15 min prior to water quenching. The resulting amorphous alloys were vacuum-sealed and annealed at a temperature of 493 K for different durations (up to 300 min) to obtain varying percentages of crystallinity. The amorphous/crystalline nature of these heat-treated specimens was examined by X-ray diffraction (XRD), differential scanning calorimetry (DSC) and transmission electron microscopy (TEM).

Because the current processing limitations only allow for the production of maximum 4 mm diameter rods that are fully amorphous, a non-standard test sample was used for impact testing. However, it is noted that the primary interest of this work is in *understanding the relative change in impact toughness*

---

† Even if the dislocation activity is insignificant (which can be anticipated due to the intermetallic nature of crystallized phases), higher grain sizes can lead to higher γ because of the increased propensity for crack deflection.

with crystallinity. Great care was exercised to ensure the specimens tested were geometrically identical so that the results can be compared in a straightforward manner. Cylindrical specimens of dimensions 22 mm in height and 4 mm in diameter were prepared and notched (notched depth ≈ 0.3 mm) in a low speed diamond saw prior to testing. The impact tests were carried out in Izod configuration in a tabletop, instrumented Charpy test machine. The drop hammer of the impact machine was calibrated to impart energy of 2.73 J at a velocity of 2.49 m/s and the resultant load vs displacement/time history was recorded. Impact toughness was calculated by taking the area under the load–displacement curve up to the maximum load, and dividing it by the unnotched cross-sectional area of the specimen. The fractured samples were gold coated prior to examining the fracture details in a scanning electron microscope (SEM). Also, rectangular beams of dimensions $1.5 \times 3.5 \times 28$ mm^3 were cut from the cylindrical rods and mounted in a dynamic mechanical thermal analyzer (DMTA) in a three-point bend configuration. The in-phase modulus, E', and the damping constant, $\tan \delta$, of the materials were measured by applying an oscillatory load at radial frequencies ranging from 6.28 to 628 rad/s.

3. RESULTS

3.1. Material characterization

The bulk amorphous glass specimens of composition $La_{55}Al_{25}Cu_{10}Ni_5Co_5$ were uniformly cylindrical with > 99% relative density. The XRD pattern as shown in Fig. 1 does not reveal any significant peak for the as-quenched material, indicating that it is fully amorphous. The diffraction patterns of specimens after annealing heat treatment did show peaks corresponding to crystallizing phases in the microstructure. The intensity of the peaks was observed to increase with the duration of heat treatment.

The DSC curves of the as-quenched and six other specimens heat-treated to various time intervals at 493 K are shown in Fig. 2. Results show that the amorphous material in the present system exhibited a glass transition temperature, T_g, at ∼482 K and was followed by a wide supercooled liquid region with a temperature interval, ΔT_x, of 83 K. The onset of crystallization, T_x, concurrent with the first appearance of a crystallization peak ($\Delta H_x = 3.85$ kJ/mol) occurred at the temperature of about 565 K [26]. However, with the present annealing schedule, no appreciable change in T_g was observed in the partially amorphous samples, although T_x showed a decreasing trend for specimens annealed for 30–140 min and increased again for a longer duration of 300 min. The same trend was observed for ΔT_x with 72 K for the specimen annealed for 30 min, decreased to 50 K for 140 min, and
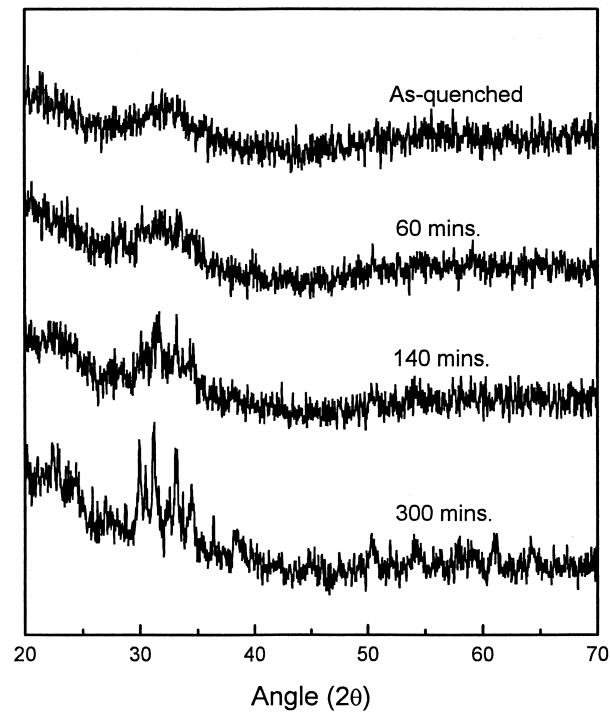
Fig. 1. X-ray diffraction patterns of the amorphous alloy annealed at 493 K for various times.

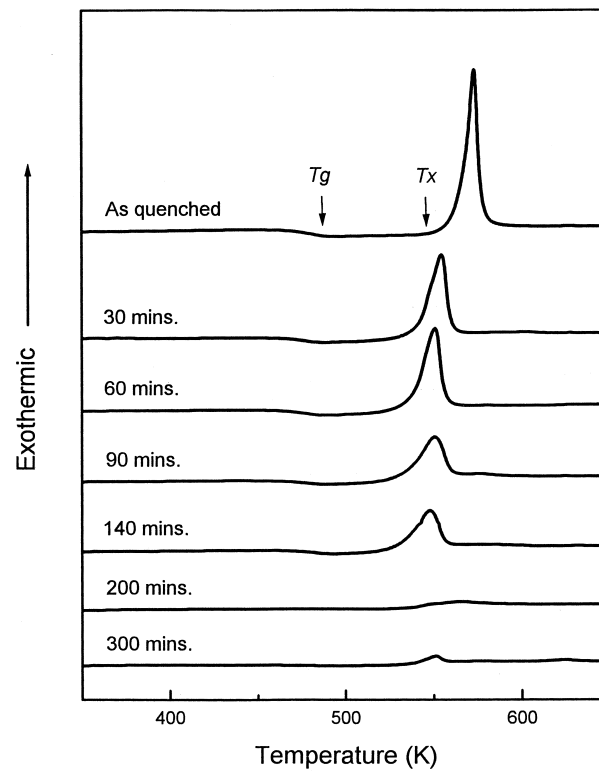Fig. 2. DSC curves of the amorphous alloy annealed at 493 K for various times.

Table 1. DSC results of water-quenched $La_{55}Al_{25}Cu_{10}Ni_5Co_5$ samples with different duration of heat treatment at the heating rate of 0.67 K/s

Duration (min)	T_g (K)	T_x (K)	T_p (K)	ΔT_x (K)	Crystallinity (%)
0	482.22	565.42	572.34	83	0.00
30	479.06	551.11	565.12	72	18.41
60	478.65	538.03	550.82	59	19.10
90	479.44	533.90	550.71	54	34.26
140	480.88	530.43	547.43	50	49.69
200	478.50	536.57	561.71	58	88.15
300	477.95	537.78	550.60	60	93.15

increased again to 60 K for the specimen annealed for 300 min.

The computed percentage of crystallinity, χ from the DSC results (Table 1) shows that χ increases with increasing annealing time, from 18.4 to 93.2% upon annealing to 30 and 300 min, respectively. A plot of χ against the annealing time (Fig. 3) indicates that initially χ increases exponentially with annealing time. This was followed by a regime wherein longer annealing times (e.g. 200–300 min) had no significant change in the crystallinity of the material.

The TEM image of the microstructure indicated nanosized crystallites (~ 10 nm) distributed uniformly in an amorphous matrix in the sample heat treated for 60 min [Fig. 4(a)]. The corresponding diffraction pattern showed a few fine sharp rings coexisting with the amorphous diffuse ring, indicating the presence of a substantial amount of amorphous phase. This was in accordance with the DSC results of 19.1% crystallinity (Table 1). It was observed that the crystallites coarsened upon increasing the duration of heat treatment from 90 to 300 min [Figs 4(c) and (e)]. The corresponding diffraction patterns of these specimens revealed fine spots because of increases in crystal size resulting from increasing durations of heat treatment. The diffraction pattern from the specimen heat treated to 300 min showed a few large spots indicating large crystal sizes.
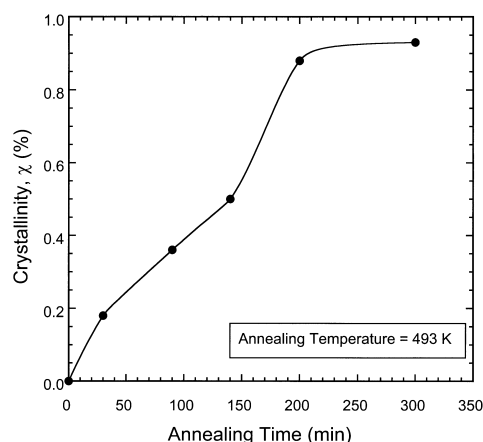

Fig. 3. Crystallinity, χ, of the bulk glass as a function of the annealing time at 493 K.

3.2. Impact properties and fracture

A typical impact load–displacement curve for the alloy system is shown in Fig. 5(a). The curve had distinct peaks, some of which are presumed to result from resonant vibrations of the specimen at the impact fracture [15]. A maximum load of 0.6 kN corresponding to an impact fracture stress (calculated on the basis of the unnotched cross-sectional area) of 46 MPa was measured for the fully amorphous material. With increasing χ, the peak impact load dropped considerably with a minimum at $\chi \sim 50\%$ and increased slightly with further crystallization to $\chi \sim 93\%$ [Fig. 5(b)]. The time to reach maximum load shows a trend that is commensurate with the peak load [Fig. 5(b)]. The time taken for complete fracture of the specimens was ~ 0.4 ms and was observed to be independent of χ.

The impact toughness, γ, as a function of χ of the material (Fig. 6) also indicates a similar trend. Here, all the data are normalized with respect to the as-quenched (or fully amorphous) material's impact toughness, γ_b ($= 9.43$ kJ/m^2), which also happens to be the highest γ measured. A precipitous drop in γ (to 2.85 kJ/m^2) was observed upon partial crystallization ($\chi \sim 19\%$). With increasing χ, γ decreases further and reaches a minimum of 0.79 kJ/m^2 at $\chi \sim 50\%$. Further increase in χ (to $> 80\%$), resulted in an increase in γ to 1.37 kJ/m^2. Note that this increase is significant ($\sim 73\%$) with respect to the minimum γ observed in the γ vs χ curve. This fact was highlighted through the inset of Fig. 6, where γ is normalized with γ_{min}.

Macroscopic observation of the fractured surfaces reveals two distinct regimes of fracture in the specimens (Fig. 7). The material in the fully amorphous state shows a very jagged fracture surface. The surface roughness was very high near the notch root and decreases progressively away from the notch. The area fraction of the jagged surface decreased with increasing χ and was accompanied by increased area fraction of cleavage fracture. In materials with χ greater than 35%, the fracture was totally featureless at the macroscopic level, typical of cleavage fracture in brittle materials such as glass or ceramics.

SEM examination of the jagged fractured surfaces shows vein-like fracture typically observed in tensile fracture of bulk metallic glass [27, 28]. It was

also observed that the veins were much deeper in the very jagged surfaces near the notch root [Fig. 8(a)], similar to the ductile mode of failure observed in many metals. The depth of the veins became shallower with distance away from the notch root [Fig. 8(b)]. With increasing crystallinity, the veins tended to become shallower at the notch root [Fig. 8(c)] and very often both shallow and deeper veins could be observed [Fig. 8(d)]. On the other hand, the cleavage regions were microscopically flat. However, observations at high angle tilt of 60° did reveal isolated pockets of vein-like frac-

ture [Fig. 8(e)] in a cleavage matrix. In the nearly fully crystalline material, although no vein-like pockets were observed the fracture was significantly more tortuous and intergranular [Fig. 8(f)].

3.3. Dynamic properties

Typical variation in the measured in-phase modulus, E', and the damping constant, $\tan \delta$, with the material crystallinity, χ was shown in Fig. 9. The range of ω over which the DMTA measurements were made (6.28–628 rad/s) is small and probably
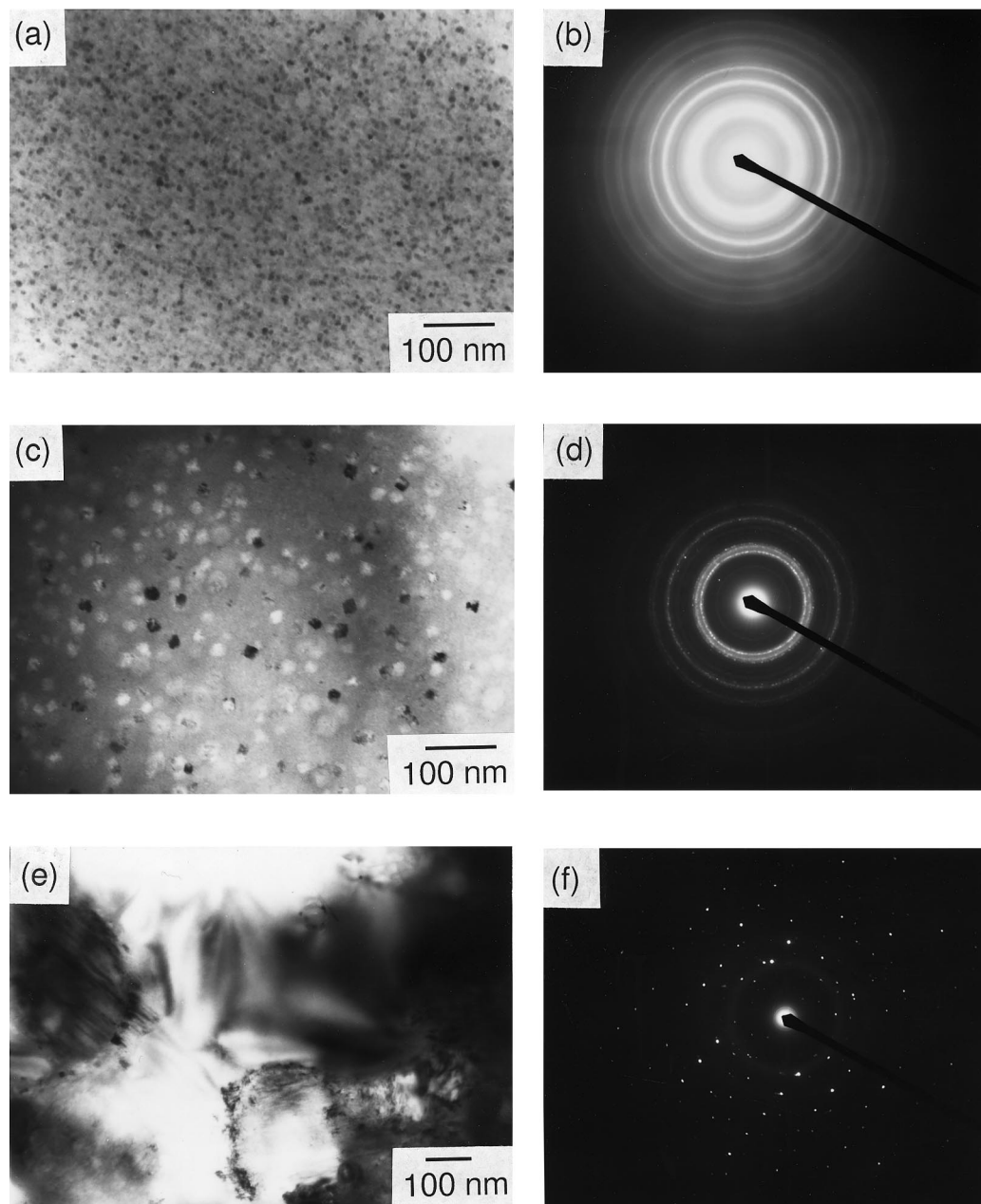

Fig. 4. TEM micrographs of the metallic glass annealed at 493 K for: (a) 30 min; (c) 90 min; (e) 300 min. (b), (d), (f) Respective diffraction patterns.

confined to the higher side of the frequency spectrum. As a consequence of this small range, no appreciable influence of ω on both the E' and the $\tan \delta$ was observed. The E' increases with χ, from ~ 45 GPa in the fully amorphous material to 54 GPa in the material with $\chi \sim 93\%$. Correspondingly, $\tan \delta$ decreases with increasing χ, indicating the lowered viscous nature of the material. The DMTA results are analyzed within the framework of the Maxwell model for linear viscoelastic material under dynamic loading [29]. The purpose of using this simple model is to highlight the variation in macroscopic relaxation behavior that occurs with crystallization. Additionally, it is worth noting that such a model has been successfully used to rationalize the uniaxial stress–strain response of Pd-based metallic glass [30]. According to the Maxwell model, the complex modulus of the material, E^*, is given by

$$E^* = \{(E')^2 + (E'')^2\}^{1/2} \tag{1}$$

where E'' is the loss modulus (given by the relation $\tan \delta = E''/E'$). For the as-quenched material, the

E^* was measured to be 47 GPa which increases nominally to 48 GPa upon partial crystallization ($\chi = 18.4\%$). The modulus increased steeply to 53 GPa upon further crystallization to $\chi \sim 36\%$. However, no significant increase was observed upon further crystallization and a maximum of 56.5 GPa was recorded in the material with $\sim 93\%$ crystallinity.

The complex modulus E^* is related to the elastic modulus, E, of the material through the following expression:

$$E = E^*(1 + \tan^2 \delta)^{0.5}. \tag{2}$$

Since the measured values of $\tan \delta$ are small (ranging from ~ 0.03 in the glass to 0.003 in the crystalline material), E is almost equal to E^*. Independent measurements of the elastic modulus by the instrumented indentation technique showed excellent correlation with the DMTA results (44 GPa in amorphous glass and 54 GPa in the nearly crystalline alloy). This $\sim 20\%$ increase in E^* due to nearly full crystallization over that of the base amorphous alloy is similar to a gain of $\sim 30\%$ observed in a Zr-based alloy where its Young's modulus changed from 88 GPa for the glass sample to 116 GPa for a fully crystalline sample [31].

The viscosity of the material, η, was computed from the following relation [29]:

$$\eta = E/(\omega \tan \delta). \tag{3}$$

Variation in η as a function of the crystallinity in the specimen is shown in Fig. 10. For any given ω, η increases with increasing χ. The increase was gradual until $\chi \sim 36\%$ and an abrupt increase was observed at around $\chi \sim 50\%$. Further increase in the crystallinity had no significant change on viscosity although a marked drop was measured in the nearly full crystalline material.
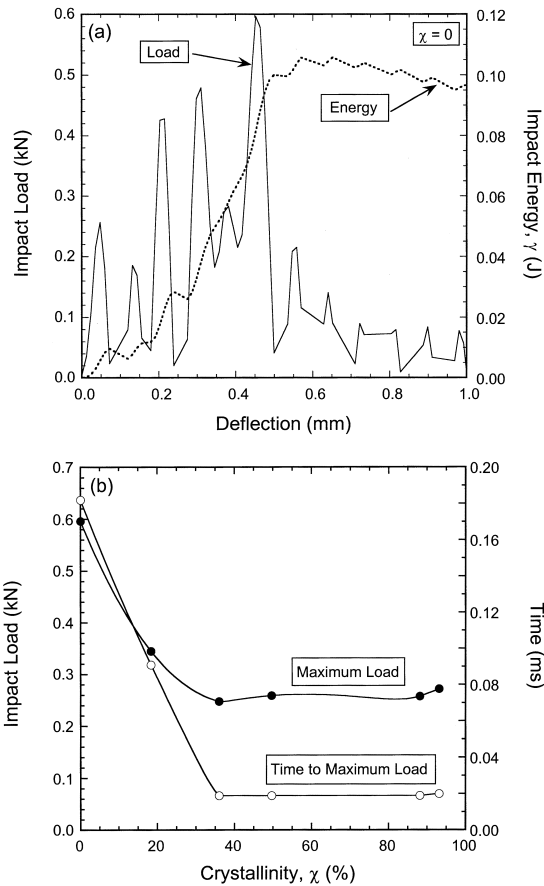

Fig. 5. (a) Typical plot of load and energy vs deflection observed during the impact test. (b) Variation of peak impact load and time taken to reach peak impact load as a function of the crystallinity.
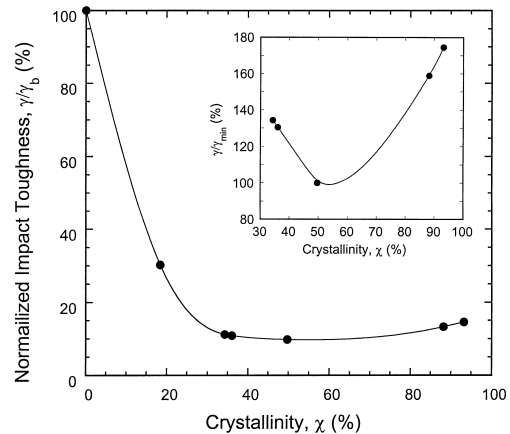
Fig. 6. Variation in impact toughness, γ (normalized with the impact toughness of the as-quenched alloy, γ_b), as a function of the material's crystallinity, χ. The inset shows the γ normalized with γ_{min} as a function of χ.

The effect of the applied frequency on the measured viscosity was examined in Fig. 11, by plotting η (normalized with respect to the η measured at $\omega = 6.28$ rad/s) against ω. It is seen that all the data collapse on to a single curve when plotted in this manner, irrespective of the crystallinity. Furthermore, a log–log plot was chosen to illustrate the functional relationship between η and ω. The ω range has a significant influence on the material viscosity, with η increasing by three orders of magnitude to a decrease in frequency.

4. DISCUSSION

4.1. Crystallization kinetics

Inoue and Fan [32] have stated that nanocrystallization within the amorphous phase in metallic glasses requires a two-stage crystallization process. They also indicated that it would be difficult to obtain a fully nanocrystalline material from an amorphous alloy that exhibits only a single exothermic peak, where the crystallization leads to the simultaneous formation of multiple phases [32]. The crystallization behavior of the present amorphous alloy is characterized by a single exothermic peak after a large undercooled liquid region (Fig. 2). Although, nanocrystalline phases were observed in the early stage of crystallization [Figs 4(a) and (c)], coarse phases (with grain size larger than 200 nm) were observed in the nearly fully crystallized sample [Fig. 4(e)]. The diffraction (both X-ray and TEM) results indicate that these primary nanocrystals are most likely to be some intermetallic compounds and not α-La phase, since the d-spacings do not correspond to those of the La phase.

The crystallization kinetics of metals are well described by the Johnson–Mehl–Avrami (JMA) equation. However, the crystallization kinetics of multicomponent amorphous alloys cannot be described successfully by this model [33]. Modified JMA models or grain growth type models (which assume that the as-quenched material already has a
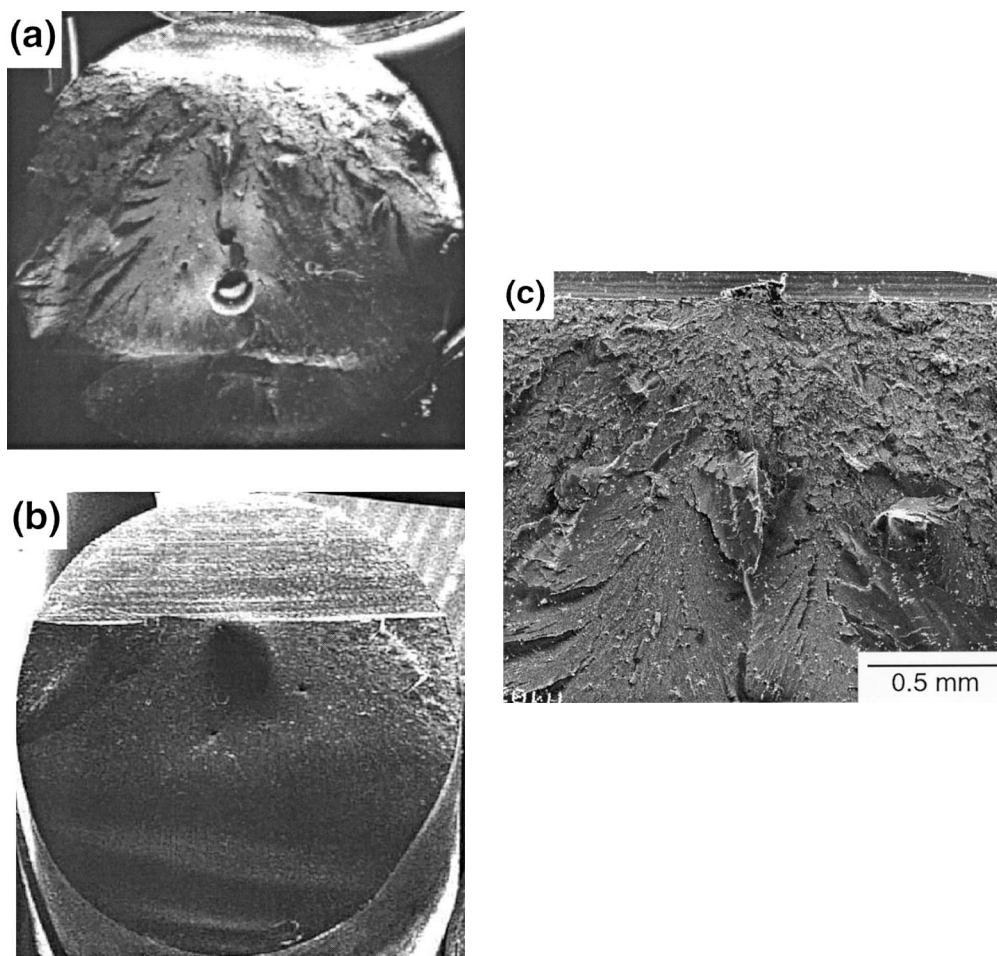

Fig. 7. Macroscopic observation of fractured surface in (a) the as-quenched specimen and (b) the specimens with a $\chi \sim 34\%$. (c) Higher magnification view of the notch root of the as-quenched specimen showing jagged fracture surface.

very fine crystalline structure) have been employed to describe the kinetics. Xing *et al.* [34] have studied the crystallization behavior and microstructure evolution of a $Zr_{57}Ti_5Al_{10}Ni_8Cu_{20}$ alloy under different annealing temperatures and attributed the deviation from the JMA model to the increasing crystallizing temperature of the residual amorphous phase with increasing χ.

Although, the crystallization mechanisms are not fully understood, it has been suggested based on the kinetic studies of nucleation and growth events [35, 36] that the nucleation in amorphous alloy occurs heterogeneously at quenched-in nuclei. The quenched-in medium range order (MRO) domains are expected to play an important role in the evolution of nanocrystalline microstructure by providing nucleation sites for precipitation of primary crystals [37, 38]. In the present study, TEM micrographs of the samples heat treated to various times do indeed reveal the presence of nanometer-sized crystallites [Fig. 4(a)] that coarsen upon further heat treatment [Fig. 4(c)]. As indicated earlier in

Fig. 3, the glass is never fully crystalline and pockets of residual amorphous glass exist even after extended periods of annealing time. The nearly crystalline alloy indicated formation of regular grained structure and precipitation of secondary crystalline phases at the grain boundaries [Fig. 4(e)].

4.2. Fracture mechanisms

The deformation behavior of amorphous metal alloys (particularly in thin ribbon form) is well studied and several reviews can be found in the literature [22–24, 27, 28]. The deformation mechanisms depend on the relative temperature (with respect to T_g), the rate of deformation, and the stress applied [22]. At low stresses (< 0.01 times the yield strength) and high temperatures ($\sim T_g$), homogeneous deformation characterized by Newtonian viscous flow occurs [22]. The inhomogeneous mode of deformation characterized by localized shear band formation prevails at low temperatures ($\ll T_g$)
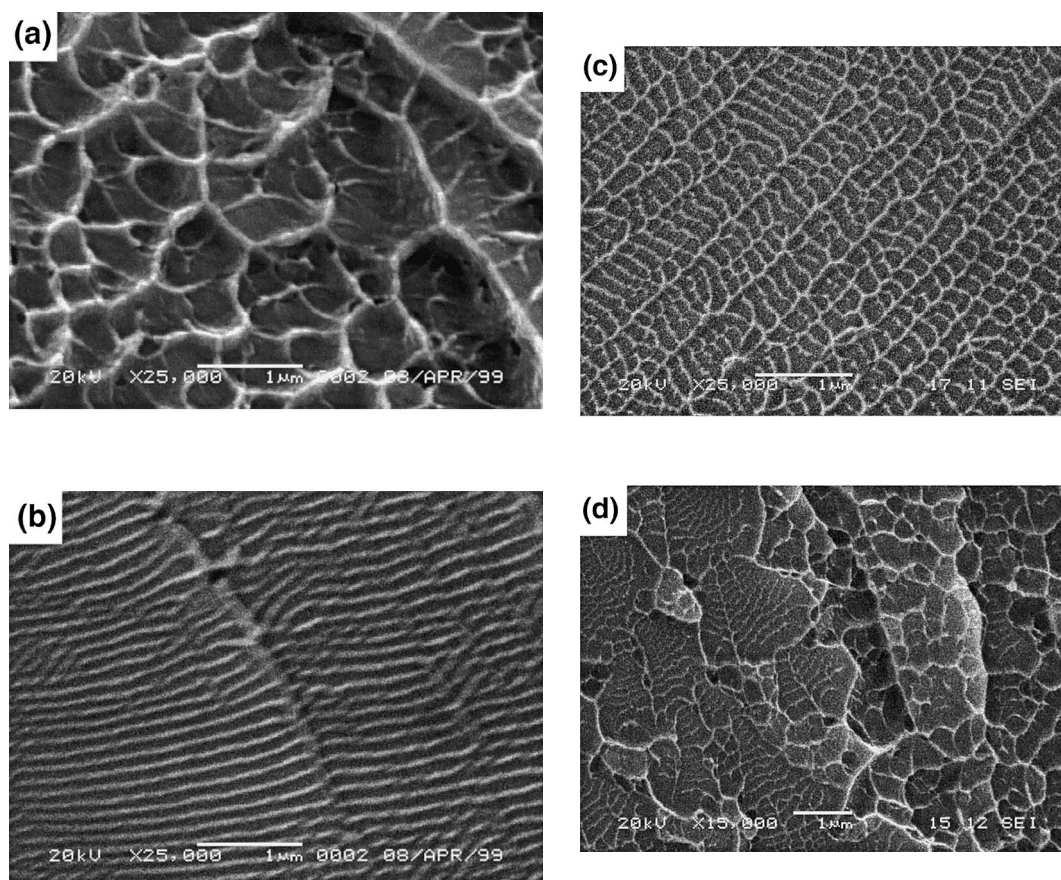

Fig. 8. High magnification fractographs in specimens with different degrees of crystallinity: typical "venous" pattern observed in the as-quenched alloy showing (a) deeper veins at the notch root and (b) shallower veins away from the notch root. (c), (d) Fracture features at the notch root in specimens with $\chi \sim 18.4$ and 34%, respectively, showing that the veins become shallower with increasing χ. (e), (f) High angle tilt images indicating cleavage fracture with sporadic residual viscous glass ($\chi \sim 50\%$) and intergranular cleavage with tortuous crack ($\chi \sim 93\%$). Arrow in micrograph (e) indicates localized melting.
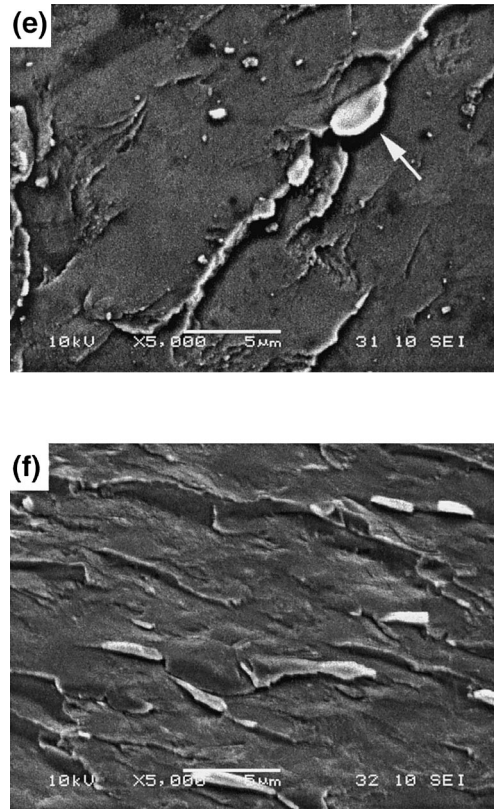
Fig. 8 (*continued*)

and high stresses or high strain rates. The shear bands are narrow (typically ranging from thickness of 5–40 nm) and experience severe plastic strains (of the order of 1000%) through viscous shearing (associated with stress-enhanced structural relaxation and adiabatic heating). The density of the shear bands dictates the overall plastic strain accommodated by the metallic glass.

In metallic glasses, because of the viscous nature of the glass, a strong dependence between γ and the imposed rate of deformation can be anticipated. Under high rates of deformation, localized melting associated with inhomogeneous flow occurs during catastrophic fracture. Infrared surface measurements by Flores and Dauskardt [39] indicate a peak temperature increase of $\sim 55\,K$ due to the plastic deformation at the
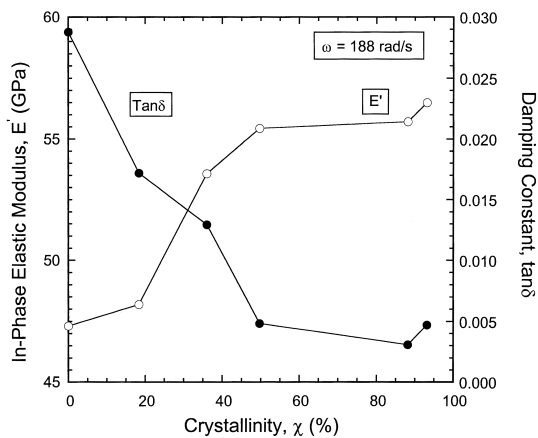

Fig. 9. Variation in storage modulus, E', and damping constant, $\tan \delta$, with the degree of crystallinity, χ, of the material (at $\omega = 628$ rad/s).
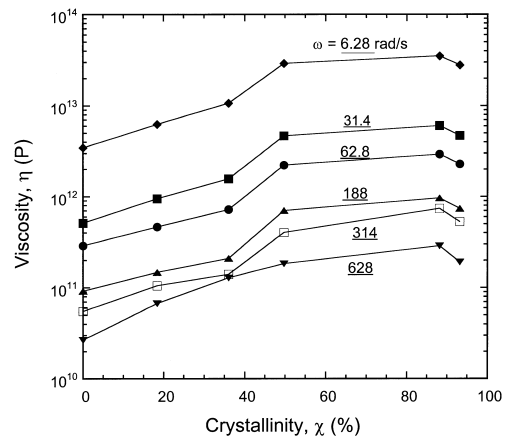

Fig. 10. Variation in viscosity, η, with the degree of crystallinity, χ, for various radial frequencies, ω.
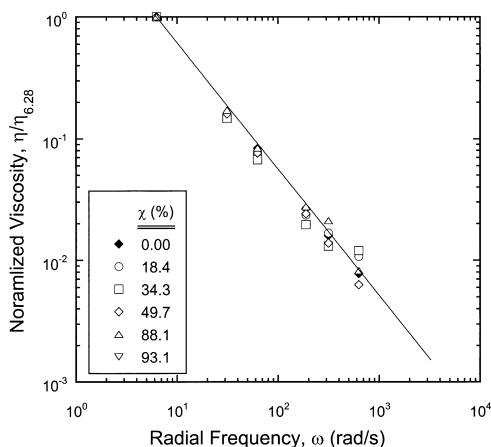
Fig. 11. Variation in viscosity, η (normalized with respect to the η measured at $\omega = 6.28$ rad/s) as a function of the applied radial frequency, ω.

crack tip. Gilbert *et al.* [18] observed that the $Zr_{41.2}Ti_{13.8}Cu_{12.5}Ni_{10}Be_{22.5}$ glass fractured with emission of bright sparks upon impact testing in air whereas no sparks were seen when tested in nitrogen atmosphere. They argued that along with oxidation induced heat generation, intense heat was also generated due to plastic work. Observations of highly localized deformation in the glass and surface remelting provide support for this argument. They concluded that heat emitted by the deformation was enough for local temperature to exceed 935 K, at which the metallic glass liquefies. In the current work, no visible sparks were observed during impact testing of the amorphous alloy. However, fractographic observations do indicate a localized melting phenomenon [Fig. 8(e)].

The superior strength of partially crystallized materials vis-à-vis fully amorphous metals has been attributed to the mechanism of nanocrystalline particles acting as barriers to the shear bands [40]. Typically, the strength increases with increasing χ up to a critical value, whereas elongation to failure remains unaltered [21]. Inoue and co-workers [21] have observed a maximum in strength for partially crystallized structures of both Zr–Ti–Ni–Cu–Al alloys as well as Al–Ni–Y alloys. A maximum in strength indicates that there is an optimum size of the crystalline particles. (Aside, it is interesting to note that this mechanism appears to be analogous

to the hardening mechanisms in precipitation strengthened Al alloys in a number ways.) Beyond the maximum, a precipitous drop in both strength and elongation with increasing χ were noted [21]. No mechanistic explanations were offered for this drop in Zr alloys. For the case of the Al–Ni–Y system, Kim and Hong [41] proposed a model for the ductile–brittle transition, which assumes the material becomes brittle when the solute (Y) concentration in the Al particle/amorphous matrix interlayer reaches a critical value.

Both microscopic and macroscopic fractographic observations made in the present work are in good agreement with the deformation and ductile–brittle transition mechanisms. The high strain rate due to impact loading and the high stress intensity at the notch root should promote localized shear band deformation whereas farther away form the root, the stresses and the rates are much lower allowing for homogeneous deformation. The observation of vein pattern (a result of the localized flow of glass within narrow bands) that is significantly deeper at the notch root than that away from the notch root in the fully amorphous alloys [Figs 8(a) and (b)] confirms this. With increasing crystallinity, the veins become much shallower at the notch root itself [Fig. 8(c)], indicating lesser propensity for shear band deformation, reducing to insignificant amounts when the crystalline volume fraction reaches $\sim 35\%$ [Fig. 8(d)]. Further crystallization appears to lead only to brittle fracture of the material.

Recently, Conner *et al.* [42] have studied the $Zr_{57}Nb_5Al_{10}Ni_{12.6}Cu_{15.4}$ metallic glass matrix composites reinforced with W, WC, Ta, and SiC particles and indicated that the toughness of the composite system (as indicated by the area under the uniaxial stress–strain curve) increased by $\sim 50\%$. This increase in toughness was attributed to the restriction of shear band propagation by the reinforcement particles, resulting in the promotion of multiple shear band formation within the amorphous matrix [42]. Clearly, this result indicates that large *extrinsic* reinforcements assist in "homogenizing" the plastic deformation. Precipitation hardening mechanism analogy suggests that finer particles should, in principle, promote more homogenization and in turn should lead to higher toughness. Our toughness measurement as well as that of other researchers suggests to the contrary†. The marked decrease in toughness of nanocrystalline precipitate-amorphous matrix composites suggests that crystallization decreases the propensity for shear band formation. This may be due to the solute redistribution during crystal growth that possibly increases the melting temperature of the diffusion zone and the amorphous matrix [34]. Since increasing melting temperature generally leads to higher viscosity, the average viscosity of the residual amorphous matrix can be assumed to increase with

---

† Note that the composites tested by Conner *et al.* [42] were manufactured by a processing approach different from that used in the present study. In addition, several other factors such as the sizes, interfacial conditions, and the relative differences between the matrix and the reinforcement could play a significant role in influencing the shear band nucleation and propagation and in turn the toughness under either static or dynamic loading conditions.

increasing χ. This increase in viscosity leads to suppression of shear band nucleation and hence promotes brittle fracture.

4.3. Role of viscous deformation

While the preceding section highlights some of the possible *micromechanims* for the fracture transition, this section addresses the variation in the macroscopic viscoelastic attributes of the metallic glass with crystallization and how they might influence the ductile–brittle transition. This particular aspect of this study was motivated by the observation of time taken to reach the peak load, which dropped dramatically with the increase in crystallinity [Fig. 5(b)], despite only a subtle change in the fracture morphology [Figs 8(a)–(d)]. Recently, Kato et al. [30] have proposed a model that includes stress-induced structural relaxation for viscoelastic deformation of amorphous metals. They have shown that the model quantitatively reproduces the experimentally observed stress-overshoot with increasing strain rate in a $Pd_{40}Ni_{10}Cu_{30}P_{20}$ bulk metallic glass [31]. This conclusion suggests that it may be possible to understand the ductile–brittle transition by an assessment of the changes in the material's viscoelastic nature.

The key material property that captures a viscoelastic material's response under dynamic loading condition is the characteristic relaxation time, τ (defined as η/E) [29]. The extent of stress relaxation due to viscous flow for a given material will depend on the relative difference between τ and t, the time of loading during experimentation. When $t > \tau$, there is time for viscous deformation to take place whereas for $t < \tau$, the materials behaves elastically.

In the $La_{55}Al_{25}Cu_{10}Ni_5Co_5$ system under investigation, DMTA experiments show that both E and η are strongly coupled to the degree of crystallinity in the alloy (Figs 9 and 10). With increasing χ, the

in-phase modulus, E', increases while the damping constant, $\tan \delta$, decreases. The initial steep drop in $\tan \delta$ and in turn in η, could possibly be attributed to the solute redistribution (as discussed in the preceding section) and impediments created by the crystallizing phases to some of the thermally activated processes such as diffusion. Also, a significant decrease in free volume with crystallization also manifests in a rapid increase in viscosity [22, 23]. A slight increase in $\tan \delta$ upon nearly full crystallization is not fully understood, but is very likely due to the activation of residual amorphous and viscous elements at the grain boundaries similar to that suggested by some of the literature on ceramics [43–48].

The relaxation time as well as the impact toughness were plotted in Fig. 12 as a function of the material's crystallinity. It is apparent that the impact toughness absorbed decreases as τ increases. While the measured τ is small in the as-quenched material, it increases significantly upon crystallization. By graphing the observed fracture mode, three distinct regimes of material behavior can be delineated.

For the as-quenched alloy, contribution of the viscous deformation to the overall material behavior is significant because of the low τ. Hence, extensive shear band nucleation and propagation is facilitated, leading to high toughness values. Observation of uniform and deep veins on fractured surfaces [Figs 8(a) and (b)] supports this hypothesis. The veins are much deeper, coarser at the notch root and are shallower away from the notches. This is possibly because of the high stress concentration at the notch root at the instance of loading, decreasing away from it and with the time of contact.

Upon partial crystallization, the amorphous alloy gets embrittled because of a sharp rise in τ. Densification, solute redistribution, and loss of free volume upon annealing (discussed in detail in the preceding section) are the possible reasons for the increase in viscosity and in turn in τ upon crystallization. Since the loading rate is such that the time is not sufficient for extensive viscous shear band formation, extensive plastic deformation through such mechanism is limited. Furthermore, the crystalline phases in the microstructure could be acting as barriers for shear band propagation, exacerbating the loss in toughness. The fracture morphology tends to be a combination of featureless cleavage fracture with shallow and less-dense vein structure [Figs 8(c) and (d)].

When the material is nearly full crystalline, a marked increase in the toughness is observed. This is followed by a perceptible shift in the fracture morphology to that of crystalline intergranular cleavage. The variation in crystallographic cleavage planes from one grain to another leads to an increase in the crack-path tortuousity. With
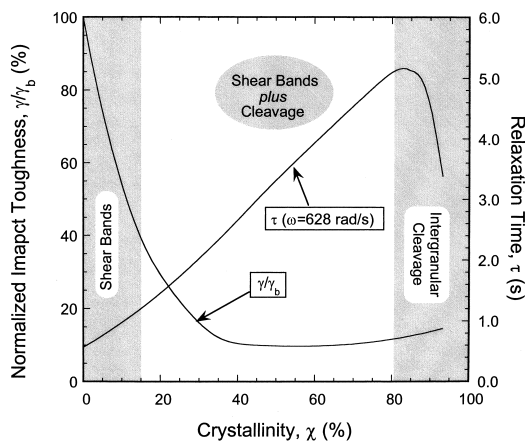
Fig. 12. Impact toughness and relaxation time as a function of material crystallinity, χ.

increased crack deflection, crack-tip shielding becomes more effective, and hence the measured toughness of the material increases [49]. The observation of appreciable increase in the fracture surface roughness [Fig. 8(f)] supports this hypothesis. It appears, however, that the contribution from the dislocation-based plastic deformation mechanisms to the overall toughness is limited, as cleavage facets are featureless. The intermetallic nature of the crystalline phases is perhaps the reason for this.

Although the hypothesis for the ductile–brittle transition in bulk metallic glasses upon crystallization is supported by the measurements and observations made in this study, further research is necessary to validate them. In particular, crack-tip TEM studies to precisely identify the micromechanisms of deformation and fracture, coupled with experiments to determine the rate dependence of toughness, are essential for developing a clearer understanding.

5. SUMMARY

In this investigation, a detailed study on the effects of crystallization on the impact toughness of a La-based bulk amorphous alloy has been presented. Experimental results confirm ductile–brittle fracture transition, associated with a precipitous drop in the impact toughness, upon partial crystallization of the amorphous alloy. This transition was associated with a vein to featureless-cleavage transformation in the fracture morphology. However, the material appreciably recovers some of its impact toughness upon annealing to a nearly full crystalline state. Increased crack-path tortuousity leading to increased surface roughness was thought to be the possible reason for the higher energy absorption. The transition in the toughness characteristics and the fracture morphology has been rationalized by considering the variation in the viscoelastic characteristics, particularly the characteristic relaxation time, with crystallization. On the basis of the relative differences between the relaxation time with crystallization, three distinct regimes of fracture are identified, which appear to agree well with the observed variations in fracture morphology.

REFERENCES

1. Li, J. C. M., in *Rapidly Solidified Alloys*, ed. H. H. Liebermann. Marcel Dekker, New York, 1993, p. 379.
2. Inoue, A., Zhang, T. and Masumoto, T., *Mater. Trans., JIM*, 1990, **31**, 177.
3. Zhang, T., Inoue, A. and Masumoto, T., *Mater. Trans., JIM*, 1991, **32**, 1005.
4. Peker, A. and Johnson, W. L., *Appl. Phys. Lett.*, 1993, **63**, 2342.
5. Inoue, A., Zhang, T., Nishiyama, N., Ohba, K. and Masumoto, T., *Mater. Sci. Engng A*, 1994, **A179/A180**, 210.
6. Inoue, A., Shinohara, Y. and Gook, J. S., *Mater. Trans., JIM*, 1995, **36**, 1427.
7. Inoue, A., Nishiyama, N. and Matsuda, T., *Mater. Trans., JIM*, 1996, **37**, 181.
8. Inoue, A., Zhang, T. and Zhang, W., *Mater. Trans., JIM*, 1996, **37**, 99.
9. Inoue, A., Zhang, T. and Takekuchi, A., *Mater. Trans., JIM*, 1996, **37**, 743.
10. Inoue, A. and Zhang, T., *Mater. Trans., JIM*, 1996, **37**, 1726.
11. Lowhaphandu, P. and Lewandowski, J. J., *Scripta mater.*, 1998, **38**, 1811.
12. Gilbert, C. J., Ritchie, R. O. and Johnson, W. L., *Appl. Phys. Lett.*, 1997, **71**, 476.
13. Gilbert, C. J., Lippmann, J. M. and Ritchie, R. O., *Scripta mater.*, 1998, **38**, 537.
14. Gilbert, C. J., Schroeder, V. and Ritchie, R. O., *Metall. Trans. A*, 1999, **30**, 1739.
15. Inoue, A., Zhang, T. and Masumoto, T., *Mater. Trans., JIM*, 1995, **36**, 391.
16. Brown Jr, W. F., in *Aerospace Structural Metals Handbook*, Code 1224. Metals and Ceramics Information Centre, Metals Park, OH, 1989, pp. 1–30.
17. Venkateswara Rao, K. T. and Ritchie, R. O., *Int. Mater. Rev.*, 1992, **37**, 153.
18. Gilbert, C. J., Ager III, J. W., Schroeder, V., Lloyd, J. P., Graham, J. R. and Ritchie, R. O., *Appl. Phys. Lett.*, 1999, **74**, 3809.
19. Fan, C., Takeuchi, A. and Inoue, A., *Mater. Trans., JIM*, 1999, **40**, 42.
20. Xing, L. Q., Eckert, J., Löser, W. and Schultz, L., *Appl. Phys. Lett.*, 1999, **74**, 664.
21. Fan, C., Louzguine, D. V., Li, C. and Inoue, A., *Appl. Phys. Lett.*, 1999, **75**, 340.
22. Spaepen, F. and Taub, A., in *Amorphous Metallic Alloys*, ed. F. E. Luborsky. Butterworth, London, 1983, p. 231.
23. Davies, L., in *Metallic Glasses*, ed. J. J. Gilman and H. Leamy. ASM, Metals Park, OH, 1978, p. 190.
24. Xing, L. Q., *Mater. Sci. Engng*, 1997, **A226–228**, 874.
25. Inoue, A., Nakamura, T., Sugita, T., Zhang, T. and Masumoto, T., *Mater. Trans., JIM*, 1993, **34**, 351.
26. Lu, Z. P., Goh, T. T., Li, Y. and Ng, S. C., *Acta mater.*, 1999, **47**, 2215.
27. Pampillo, C. A. and Reimschuessel, A. C., *J. Mater. Sci.*, 1974, **9**, 718.
28. Leamy, H. J., Chen, H. S. and Wang, T. T., *Metall. Trans. A*, 1972, **3**, 699.
29. Gittus, J., *Creep, Viscoelasticity and Creep Fracture in Solids*. Wiley, New York, 1975.
30. Kato, H., Kawamura, Y., Inoue, A. and Chen, H.-S., in *Proc. RQ-10*, Bangalore, India, August 1999, ed. K. Chattapodhyay and S. Ranaganathan, in press.
31. Wunderlich, R. K. and Fecht, H. J., *Metall. Mater. Trans.*, 1998, **29A**, 1829.
32. Inoue, A. and Fan, C., *Nanostruct. Mater.*, 1999, **12**, 741.
33. Kelton, K. F., *J. Non-Cryst. Solids*, 1993, **163**, 283.
34. Xing, L. Q., Eckert, J., Löser, W., Schultz, L. and Herlach, D. M., *Phil. Mag. A*, 1999, **79**, 1095.
35. Greer, A. L., *Acta metall.*, 1982, **30**, 171.
36. Cochrane, R. F., Schumacher, P. and Greer, A. L., *Mater. Sci. Engng*, 1991, **A133**, 367.
37. Zhang, Y., Hono, K., Inoue, A. and Sakurai, T., *Acta mater.*, 1996, **44**, 1497.
38. Fan, C. and Inoue, A., *Mater. Trans., JIM*, 1997, **38**, 1040.

39. Flores, K. M. and Dauskardt, R. H., *J. Mater. Res.*, 1999, **14**, 638.
40. Kim, Y. H., Inoue, A. and Masumoto, T., *Mater. Trans., JIM*, 1990, **8**, 747.
41. Kim, H. S. and Hong, S. I., *Acta mater.*, 1999, **47**, 2059.
42. Conner, R. D., Yim, H. C. and Johnson, W. L., *J. Mater. Res.*, 1999, **14**, 3292.
43. Davidge, R. W. and Evans, A. G., *Mater. Sci. Engng*, 1970, **A6**, 281.
44. Tsai, R. L. and Raj, R., *Acta metall. mater.*, 1982, **30**, 1043.
45. Cheeseman, C. R. and Groves, G. W., *J. Mater. Sci.*, 1985, **20**, 2614.
46. Knickerbocker, S. K., Zangvil, A. and Brown, S. D., *J. Am. Ceram. Soc.*, 1985, **6**, C99.
47. Rouxel, T. and Wakai, F., *Acta metall. mater.*, 1993, **41**, 3203.
48. Ramamurthy, U., Hansson, T. and Suresh, S., *J. Am. Ceram. Soc.*, 1994, **71**, 2985.
49. Suresh, S., in *Fatigue of Materials*, 2nd edn. Cambridge University Press, Cambridge, 1998, p. 322.